SHOCK INDUCED HOT-SPOT FORMATION AND SUBSEQUENT DECOMPOSITION IN GRANULAR, POROUS HEXANITROSTILBENE EXPLOSIVE*

by

D. B. Hayes
Sandia National Laboratories,† Albuquerque, NM 87185

ABSTRACT

Experimental and theoretical studies on granular, porous hexanitrostilbene (HNS) explosive have yielded an increased understanding of microstructural processes occurring during initiation by shock loading. Experiments involved the planar impact of HNS specimens onto fused-silica targets. Chemical decomposition liberated gaseous products, causing the pressure in the HNS to rise. Velocity interferometry measured material velocity, hence, pressure at the fused silica/HNS interface. An analysis of this pressure excursion yields chemical decomposition history. The data are interpreted in terms of a quantitative two-temperature model which considers hot spots to be formed at pore sites as a result of the irreversible work accompanying the shock. Subsequently, decomposition completion is achieved by burn fronts which propagate radially out from each hot spot at a velocity which can be determined from the bulk decomposition rate.

Analysis of the experimental data in the context of the model yields several important results: (1) the delay times corresponding to hot-spot decomposition are shorter than expected, based on extrapolated low-temperature kinetics, providing good evidence for increased chemical reactivity produced by the disruptive pore collapse process. (2) model calculations show about the same inferred hot-spot temperature for different initial porosities and particle sizes in HNS, shock-loaded to equal pressures. Thus, hot-spot decomposition times should be similar for experiments in which only particle size or pressing density is varied, provided specimens are shock-loaded to the same initial pressure. This is consistent with experimental results.

---

* This article supported by the U. S. Department of Energy under Contract DE-AC04-76-DP00789.

† A U. S. Department of Energy facility.

With regard to the propagation of the burn fronts which propagate radially from each hot spot: (3) contrary to interpretation of data on other explosives, the burn velocity does not have a strong dependence upon the prevailing pressure. Instead, in any given experiment while that pressure rises by more than a factor of two during decomposition, we see more nearly a constant burn velocity. (4) the inferred burn velocity has a very strong dependence upon the initial shock pressure. Thus, the shock is sensitizing the material in some manner. (5) the same inferred burn velocity is obtained in experiments performed on specimens pressed from bulk HNS with two different particle sizes. (6) the burn velocities which are measured are greatly in excess of classical laminar burn velocities for comparable thermodynamic conditions. The physical basis for this large (hundred fold) velocity increase is not known. Possible explanations include increased reactivity of the material by the passage of the shock and/or altered transport processes or properties which control the burn velocity.

DISCLAIMER

I. INTRODUCTION

It is generally accepted that the passage of a shock wave through a granular porous explosive leads to heterogeneous heating and to the production of hot spots which chemically decompose more rapidly than if the material had been shock heated homogeneously (Bowden & Yoffe). Hot spots, however, constitute only a small mass fraction of the shocked explosive material. Subsequent decomposition is thought to take place by the propagation of burn fronts which propagate radially from each hot spot, ultimately consuming the material (Eyring, Powell, Duffey, & Parlin). This general picture has recently provided a basis for a variety of mathematical descriptions to model both the decomposition process and mechanical behavior of the decomposing mixture (Lee & Tarver; Hayes & Mitchell; Kipp, Nunziato, Setchell & Walsh). Most descriptions of the decomposition process are empirical or semi-empirical requiring the use of at least some non-physical constants which are adjusted to obtain a good match between predicted and experimental behavior (Forest; Kanel; Wackerle, Rabie, Ginsberg & Anderson; Hayes & Mitchell; Lee & Tarver; Kipp, Nunziato, Setchell & Walsh). It is desirable to develop models which are more physically based and attempt to relate the parameters which appear in the decomposition function to independently measurable material properties.

A variety of experiments have been performed to measure the decomposition history in a high explosive after the passage of a shock. In one common technique, arrival of the shock and subsequent wave shape are observed at a witness plate or window on the rear

surface of the explosive material (Nunziato & Kennedy; Kipp, Nunziato, Setchell & Walsh). Through a series of experiments on explosive specimens of different length, evolution of a low amplitude plane shock can be measured, as it grows to a detonation. In principal, a superior technique is the use of multiple embedded magnetic or piezoresistive gauges which yield the velocity or pressure history at a number of stations, and thus make a measure of the entire flow field possible. From these whole-field data and from the equations of motion, the pressure, volume and energy histories can be deduced at each material point, and hence the decompositon history inferred (Cowperthwaite; Wackerle, Rabie, Ginsberg & Anderson; Kanel & Dremin; Anderson, Ginsberg, Seitz & Wackerle). Such an analysis has the advantage that it directly measures the decomposition history without requiring assumption of a specific analytical form for the decomposition function which must be reconciled with indirect shock data. However, the benefits have been limited by some difficulties with this experimental technique. A third technique the one considered here, involves the measurement and use of pressure transients at the impact interface after planar loading by an elastic impactor (Kennedy; Hayes & Mitchell; Mitchell & Hayes). This method has the advantage of simplicity of use and ease of interpretation up to a point; a disadvantage is the requirement for an extra assumption to extract P-V-E response which may only be warranted under special circumstances.

In this paper we examine a specific microstructural model for the shock initiation process in the porous, granular explosive hexanitrostilbene (HNS) and test the results against available

data. The data are from impact experiments in which pressure histories at the impact interface were obtained by an interferometric technique which views through a transparent impactor. Pressure excursions are used to imply the extent of the decomposition reaction. The model assumes that the majority of each grain of explosive is reversibly compressed along an isentrope and, hence, heated only to the isentropic compression temperature (Hayes & Mitchell). The substantial irreversible work which must take place in the shock front, takes the form of heat which is deposited preferentially in the vicinities of pore sites, and thus a small fraction of the material achieves a considerably elevated temperature. The hot spots thus formed must chemically decompose leading to a measurable delay in the onset of the major pressure excursion. Subsequently, the material is supposed to decompose through the radial propagation of burn fronts from each ignited hot spot into grain interiors. The dependence of velocity of the burn front upon the thermodynamic state and shock history of the unburned explosive grain interior into which it propagates are of prime interest in this study.

This paper is organized in the following way: a brief review of the experimental technique is followed by a description and discussion of the experimental results. In the next section the specific model is developed and macroscopic observables are related to microstructural behavior. Finally, there is a discussion of the seven major findings in this study which come from comparing the model with data from experiments upon porous HNS explosive, initially shock-loaded to a pressure in the range from 1.2 - 5.3 GPa.

With regard to the hot-spot formation and decomposition, the measured delay (decomposition) times:

(i) are shorter than expected, based on extrapolated low-temperature kinetics;

(ii) don't depend strongly upon initial HNS particle size indicating hot spots are formed by dissipative processes with small-scale length/time and that hot spots remain adiabatic during their decomposition; and,

(iii) don't depend strongly upon initial explosive pressing density which is consistent with our assumption that the mass fraction of hot spots approximates the initial volume fraction of pores within the solid prior to shock loading.

With regard to the propagation of intragranular burn fronts:

(iv) the inferred burn velocity does not display a strong dependence upon the prevailing pressure, even though in any given experiment that pressure rises in excess of a factor of two between reaction initiation and completion. This apparent pressure independence differs from results on several other explosives in which the decomposition rate is observed to depend strongly upon prevailing pressure (Lee & Tarver; Forest);

(v) the burn velocity is observed to have a very strong dependence upon the initial shock pressure above a threshhold of 2 GPa; both Wackerle et al. and Kanel, using direct analyses, have developed decomposition-rate laws which depend to some extent on the initial shock pressure.

(vi) the same burn velocity is inferred for specimens pressed from HNS of two different initial particle sizes, and shocked in otherwise identical experiments; and;

(vii) the inferred grain burning velocities of a few tens of meters per second, are greatly in excess (by a factor of 10^2) of the classical laminar burn velocity. These large, measured burn velocities could be attributed to increased reactivity or to enhanced transport processes in the pre-shocked material ahead of the burn fronts.

The purpose of this paper is to interpret experimental results within a consistent framework and to give guidance to further theoretical and experimental work. Our present data do not warrant a more sophisticated and precise mathematical description than given here. Of course, consistency of experimental results with any model is not sufficient reason to assert that the model accurately captures those processes which are occurring; such a comparison does, however, provide a basis for the design of future experiments which can test various hypotheses offered.

II. EXPERIMENTAL

The experiments were performed by impacting an HNS/fused-silica assembly onto a stationary fused-silica target material and observing the velocity history near the impact interface. A schematic of the experimental configuration is shown in Fig. 1. The details of the experimental configuration, measurement technique and data interpretation methods are described in detail elsewhere (Hayes & Mitchell; Mitchell & Hayes; Hayes, Mitchell & Stanton). Therefore, only a brief description is given here. The symmetric impact of fused silica on fused silica produces a particle velocity exactly one-half of the independently measured projectile velocity. Soon after impact the HNS specimen is shock-loaded and the amplitude of the shock as well as all subsequent pressure changes are transmitted to a viewing plane back in the fused-silica target. An interferometric technique (Barker & Hollenbach) is used to measure particle velocity. Because the fused-silica target assembly shown in Fig. 1 only experiences simple, right-going waves, there exists a unique one-to-one relation between pressure and particle velocity. Thus, we can determine the pressure history experienced at the HNS/fused-silica interface. These pressure histories are used in conjunction with an equation of state, which considers a non-equilibrium mixture of solid and gas (Mitchell & Hayes), to infer the decomposition history of HNS near the impact interface.

Figure 2 shows the results for experiments which were performed on a high-explosive powder designated HNS-I (Hayes & Mitchell). HNS-I bulk powder has a distribution of grain sizes which average 21 μm equivalent spherical diameter (Mitchell & Hayes).

Experimental conditions are elaborated in Table 1. At the lowest impact pressure (1.25 GPa in experiment G1) the shocked state is quiescent with no observable reaction. At the highest impact pressure (5.28 GPa in experiment G6) a prompt decomposition is noted immediately after the HNS is shock loaded. At intermediate pressures, the records are characterized by a pronounced delay after the HNS is shocked, which we have tentatively identified as the period of time while the hot spots decompose. This delay is followed by a pressure excursion which is produced by the major decomposition reaction and ends with completion. Delay time is a strong decreasing function of increasing initial impact pressure and the subsequent major decomposition reaction is noted to become more rapid for increasing impact pressure. Figure 3 shows results for experiments on HNS-I material which was pressed to initial densities of 1.39 and 1.48 Mg/m^3. These records display the same qualitative features as the other results. Finally, Figure 4 shows the records for specimens fabricated from HNS-II. This is a more coarse material with a more uniform particle size distribution; individual grains have an average equivalent spherical diameter* of 37 μm. These specimens were also pressed to an initial density of 1.60 Mg/m^3. There are the same qualitative features in these experimental records as others. Before describing the manner in which these pressure histories are analyzed to obtain the decomposition rates, it is necessary to give a fairly detailed account of the micro-structural model construction.

* The quoted equivalent spherical diameters are based on a Ziess analysis, which uses visual inspection of a photomicrograph to obtain particle size distribution. Other methods yielded different results, but the ratio of diameters for HNS-II: HNS-I always remained at about a factor of two. More details are given in Mitchell & Hayes.

TABLE 1.

Conditions for the Experiments and Results.

Shot	Specimen Density Mg/m^3	HNS Powder Equivalent Spherical Dia. μm	Impact Velocity km/s	Impact Pressure GPa	Calculated Hot-Spot Temperature K	τ_1-Hot Spot Ignition Time μs	τ_2-Characteristic Burn Time μs	Particle Burn Velocity m/s
G1[a]	1.60	21	0.503	1.25	561.	b	b	b
G3	1.60	21	0.814	2.72	920.	0.68	1.17	9.0
G4	1.60	21	0.951	3.30	1079.	0.39	0.58	18.0
G5	1.60	21	1.164	4.33	1394.	0.155	0.31	33.9
G6	1.60	21	1.346	5.28	1718.	0.076	0.21	50.0
G8	1.60	37	1.321	4.96	1607.	c	0.54	34.2
G9	1.60	37	0.932	3.34	1093.	0.42	1.03	18.0
G11	1.60	37	0.800	2.68	909.	0.72	1.68	11.0
V1	1.39	21	0.638	1.55	619.	1.56	2.10	5.0
V3	1.48	21	0.647	1.78	672.	1.7	2.92	3.6
V4	1.48	21	0.720	1.92	703.	1.01	1.00	10.5

[a] Experiment G1 had an impactor facing material of X-cut crystalline quartz. All other experiments used fused silica.

[b] No decomposition observed.

[c] Early portion of record noisy.

III. MODEL

The model for the shock compaction and subsequent decomposition of HNS considers three distinct regimes which will be discussed separately: the shock compaction process which forms the hot spots; the period of decomposition of the hot spots; and the intragranular burning which originates from decomposed hot spots.

During the shock compaction process the HNS material is assumed to be elevated to one of two temperatures. The bulk of the material in the interior of grains is considered to be compressed slowly and to experience only the isentropic compression thermal excursion. This is reasonable because the rise time for a shock propagating through a porous material is necessarily significantly longer than that of a shock propagating through the same material with no heterogeneities (Butcher, Carroll & Holt; Dunin & Surkov). The irreversible work which is performed by the shock is assumed to be preferentially concentrated in a small fraction of the material in the vicinity of pore sites. The magnitude of the irreversible work can be quantified by using the Hugoniot energy jump condition, reconciled with the partitioning of energy into the two regions.

$$\frac{P + P_o}{2} (V_{oo} - V) = W_H E(P,T_H) + (1 - W_H) E_S(P) - E(P_o,T_o) \qquad (1)$$

The left-hand side is the energy rise which accompanies the shock process assuming that the shock is steady, while the right-hand side partitions that energy rise between the cold and hot materials. The functions E and E_S are known (Hayes & Mitchell), as are the

initial and final pressures (P_o = 0 and P) and volumes (V_{oo} and V) through experiment. The mass fraction of hot material, W_H, and its temperature, T_H, are unknown.

Mader first quantified the extent of the disrupted region in the vicinity of a hot spot in a classical set of numerical simulations of a shock-induced pore closure in the liquid explosive nitromethane. He also made the qualitative observation that the volume of disrupted material was approximately equal to the volume of the pore from which the hot spot was formed. We have also performed hot-spot closure simulations using a two-dimensional hydrodynamic code (Thompson) for a variety of pore number densities and shock rise times. Our results generally agree with those of Mader. Figure 5b shows the two-dimensional temperature distribution after the collapse of a 4.2 μm diameter isolated spherical pore (initial pore shape is given in Fig. 5a) in HNS which was loaded to 3.3 GPa by a shock with rise time of 1 ns. In spite of the complex spatial temperature distribution, the extent of the highly disrupted region is approximately equal in volume to the initial pore volume. Since the temperature contour plotting interval is coarse, and the transition to background temperature gradual, this is more graphically illustrated in Fig. 5c where the volume (expressed in terms of an equivalent spherical radius) of material shock heated above a given temperature is graphed against that temperature.

Using such numerical studies for justification, we have, as an integral part of the model developed here, assumed equality between initial volume fraction of pores prior to shock arrival,

and the mass fraction of hot material just after shock passage.

$$W_H = \frac{\rho_o}{\rho_{oo}} - 1 \qquad (2)$$

The double-zero subscript denotes the porous state while the single zero pertains to the fully dense solid. The temperature distribution obtained analytically using Eqs. 1 and 2, is shown in Fig. 5c, and is in good agreement with results from the more complex method.

The second regime of the decomposition process is the interval of time while the hot spots decompose. In the experimental records, that instant when the observed mass fraction decomposed just becomes equal to W_H, is identified as the point when decomposition of hot spots is complete, and the burning mode of decomposition begins. Of course, this transition from one mode of decomposition to another is not in actuality expected to be as abrupt as we choose to calculate. This partitioning does, however, provide a convenient means of quantifying the experimental hot-spot decomposition time.

The final stage of decomposition entails burn fronts which propagate intragranularly from each hot spot. Experiments measure bulk decomposition; burn velocity is a more primitive, hence physically meaningful, quantity. In order to extract that velocity from bulk rate it is necessary to make a correction for the specific area of contact between the enlarging hot gas pockets and the unburned isentropically compressed solid. Consider a randomly dispersed distribution of ignition points with average number density equal to the number density of initial pores (with one pore per grain) within the solid, N. Ignoring compressibility

effects, it is easy to show that the decomposed fraction, x, is related to the velocity, V, with which the burn fronts have propagated radially as

$$x = 1 - \exp\left\{ - \frac{4\pi N}{3} \left[\int_o^t V dt \right]^3 \right\} \qquad (3)$$

which can be conveniently re-expressed

$$\dot{x} = \frac{3V}{r_o} (1 - x) \left[\log \frac{1}{1-x} \right]^{2/3} , \qquad (4)$$

where we have denoted the average radius of an HNS grain as r_o. Thus, the decomposition rate, $\dot{x}$, is proportional to V, the velocity of the burn fronts, with a geometric correction which accounts for the specific area of contact between the gas pockets and the isentropically compressed, unburned material. This geometric correction is very similar in its effect to those used elsewhere (see, for instance, Lee & Tarver) differing only in algebraic detail. Thus, we can use the measured bulk decomposition rate in conjunction with Eq. 4 to extract the velocity of the burn front from the decomposition history.

IV. DATA REDUCTION USING MODEL

The difficulty with the front-surface-impact technique is that insufficient information is obtained to extract P-V-E histories without invoking an additional assumption. To estimate decomposition rate from experimental results we have made the assumption here that the extent of reaction is proportional to the pressure rise at the impact interface above the initial shock pressure, P_s.

$$x = (P - P_s)/(P_f - P_s) \tag{5}$$

P_f is the final pressure. This assumption is not without explanation and has some justification: first, we have performed numerical simulations of the experiments.* For a wide range of assumed decomposition functions in these numerical simulations, a nearly linear relationship between pressure rise and extent of reaction is computed. Prototypic P-x histories calculated during numerical simulations for experiment G9 are shown in Fig. 6. Secondly, we find this process reversible in the sense that we can use the computed pressure profiles and extract the initial kinetics (to an accuracy of about 10-20%). Thus, this ad hoc assumption of linearity produces self-consistent results but leaves open the question of uniqueness.

There is a way to gain some understanding of this linear behavior other than from numerical studies. Instead of a linear

* In these calculations, at any given extent of reaction, our model of a pressure-equilibrated mixture of gaseous decomposition products and isentropically compressed solid was assumed. Each phase is assumed adiabatic. More details of this mixture model are given elsewhere (Mitchell & Hayes).

P-x relation, assume that at any instant, the HNS material at the impact face is in a P-V-x state not substantially different from that which would be produced by an equilibrated detonation wave with the extent of reaction limited by x, propagating into the HNS. We performed such calculations first by obtaining the C-J state for the partially reacted explosive, and then finding the appropriate equilibrated interface conditions through use of Riemann invariants matching pressure and particle velocity of partially reacted HNS and fused quartz at their interface. This calculation produced a remarkably linear relationship between impact interface pressure and mass fraction decomposed which is also shown in Fig. 6. Maximum deviation from linearity was 1.5% Thus, even though the wave in the interior of the HNS is unsteady, and is undergoing substantial evolution, it appears that the P-V state achieved is well approximated by assuming the state is the same as obtained behind a steady detonation on the so-called "partially reacted Hugoniot" followed by a Taylor expansion of the mixture with frozen composition. It is the code results, however, which provide empirical evidence that the linear relation is valid in the present range of experimental conditions; whether this linearity has more fundamental significance or wider application is unknown.

It must be noted that pressure measured at reaction completion does not agree well with the theoretical value using the JWL equation of state for the expansion isentrope (Hayes & Mitchell). In both experiments G4 and G9, the measured final pressure is 8.2 GPa, a value thought to be accurate to within a few percent. Theoretical pressure of 6.9 GPa comes from the analysis described

in the preceding paragraph, for x = 1, namely from matching pressure and particle velocity of the fused-silica impactor, with that of the Taylor expansion wave behind the steady, fully developed detonation. Theory and numerical simulations agree in final pressure to within 4%, immediately after reaction completion. Candidate explanations for disparity between experiment and theory include: an unsteady behavior different from that implicit in the linear P-x assumption; an experimental difficulty such as density gradients in the HNS with a larger HNS density near the surface of the specimen than supposed; or most probably an incorrect product equation of state, hence erroneous CJ pressure, volume and/or expansion isentrope.

To reduce data we have fit a new expansion isentrope with an ideal gas law which connects the known C-J point (P_{CJ} = 20 GPa, V_{CG} = 0.463 m^3/Mg) and the 8.2 GPa, V = 0.738 m^3/Mg experimental datum measured on G4 and G9. Thus, we give precedence to our own experimental measure of the product equation of state.

Records were reduced using Eq. 5. Given the resultant decomposition histories, it remains to interpret them within the framework of the proposed model. Examine Fig. 7 where the decomposition history is shown for experiment G9. The interval $0 < t < 0.42$ μs is the period of time required for the decomposed mass fraction to achieve the mass fraction supposed to reside in the hot spots; W_H = 0.087. This is the delay time which is denoted τ_1 in Table 1. The subsequent portion of the history, corresponding to decomposition through burning, is fit with a numerical integration of Eq. 4, with the parameter, $\tau_2 = r_o/V$, chosen as a best-fit value of 1.03 μs. Each experimental record was treated in a similar way with results tabulated in Table 1.

It should be noted that any reasonable interpretation of the experimental records require postulating some delay time. If the analytical fit (Eq. 4) for the burning portion of the decomposition is extrapolated to earlier times and hence smaller values of x, say to less than 0.01, there still remains an unaccounted-for interval of time between initial shocking and decomposition beginning. Thus, potentially other delay times might be argued for, based on other models, but some delay would always remain.

V. RESULTS AND DISCUSSION

Figure 8 shows the calculated hot-spot temperature as a function of initial porosity. Since there is no scale length or time assumed in Eqs. 1 or 2, results are independent of particle size. This was also the case in numerical simulations of hot-spot closure, where artificial viscous stress excited by the gross hole closure was very small; the majority of the dissipation came from the shocks produced by the collisions of the imploding surfaces. Neither do the calculated hot-spot temperatures depend significantly upon the initial porosity. This result can be interpreted as indicating that the effect of increased irreversible work, which is performed on the lower initial density material, must be distributed over a proportionately larger mass fraction (see Eq. 2).

The delay time data can provide several critical tests of these model results. Experimental results on Fig. 9 show that all measured delay times fall on a single smooth curve. Notice the independence of delay time on grain, hence pore size (HNS-I vs. HNS-II at ρ_{oo} = 1.60 Mg/m^3). Therefore, data do not contradict the assumption made in the calculation of hot-spot temperatures; that the dissipative processes responsible for hot-spot formation do not contain a scale length or scale time which is large compared with the pore radius or collapse time, respectively.

For several reasons, the best side-by-side comparison of this independence of grain size comes from experiments G4 and G9. First the experiments were performed at almost exactly the same pressure, making comparison easy. Also the records are very high quality, being among the best obtained. It was seen in Fig. 9

and in Table 1 that the measured delay times for these two experiments were almost equal. Figure 10 graphically demonstrates that fact in that the early portion of the two decomposition histories are nearly identical.

The observed particle size independence of hot-spot decomposition time is also evidence that those hot-spots remain adiabatic during that period. Based on thermal diffusivity measured at standard conditions, this is expected by a rather wide margin. There have, however, been some large transport-property values measured in shock-loaded organic materials (Bloomquist and Sheffield) so the possibility exists that standard properties don't pertain and that adiabaticity is a marginal assumption. To support this latter view, there have been some decreases in shock sensitivity in extremely fine-grained HNS material at low pressure and long pulse width (Schwarz). Unfortunately, if these prove to be due to lack of hot-spot ignition, the effect of dissipation mechanism length or time scale, which can affect the spatial extent of the hot spot during its formation may be confounded with subsequent thermal diffusion time scale, which can affect the persistence time of hot spots once produced, to give them time to decompose.

Figure 11 shows the measured delay time, τ_1, as a function of the calculated hot-spot temperature, T_H. As expected, there again is a consistent dependence of delay time on T_H which appears to be independent of grain size. Note that delay time might also be independent of initial pressing density (G-series [circles on Fig. 11] vs. V-series [non-circles]), although this is somewhat speculative since the calculated hot-spot temperature ranges for each series do not overlap.

Delay times are short which is evidence that the pore-collapse process significantly increases HNS reactivity. Figure 11 shows the calculated delay time assuming extrapolated Arrhenius kinetics, $A = 1530\ \mu s^{-1}$, $E^{\ddagger}/k = 15300$ K (after Rogers), which have been measured at lower temperature. It is obvious that the measured delay times are considerably less than those that would be anticipated by extrapolation of these low-temperature kinetics to these temperature regimes. In fact, if an attempt is made to fit the observed delay times with a thermal explosion model, the Arrhenius kinetics must be modified to the extreme values of $A = 110\ \mu s^{-1}$, $E^{\ddagger}/k = 5700$ K to achieve the agreement shown on the figure as the dashed line.

Several important insights follow from the measured burn velocities. An inspection of the particle velocity histories, which were measured in the experiments on HNS-I pressed to an initial density of 1.60 Mg/m^3, makes it obvious that the prevailing pressure is not the dominant variable in determining decomposition rate. Examine, for instance, Figure 2 at the particle velocity amplitude of 0.5 km/s, which corresponds to a prevailing pressure of 5.8 GPa. At this value of pressure the decomposition rates are markedly different, being about 0.8 μs^{-1} at this instant for experiment G3 and 5 μs^{-1} for experiment G6; a factor of six difference in rate. A comparable spread in rates is observed in comparisons with these and other records at other amplitudes. Even during an individual experiment, pressure rise doesn't seem to markedly affect rate. The best example is experiment G9 where pressure rises from 3.3 to 8.2 GPa during decomposition

yet the history is very well fit by a constant velocity burn (see Fig. 7). We have chosen to reduce each record assuming a constant velocity, because the accuracy of the data do not warrant a more detailed treatment. It is possible in some of the records that the velocity could vary by 30% and we could not detect that variation. However, the possibility of a strong pressure dependence can be eliminated.

Figure 12 shows that the inferred burn velocity is an extremely strong function of the initial shock pressure. Again, to within the scatter in the data, it appears that very similar burn velocities are obtained, independent of particle size and initial pressing density.

Since the burning occurs in the shock-compacted solid, there is no opportunity for intergranular convective heat transfer, such as occurs in packed beds. Also, pressures are high, hence there is essentially perfect thermal contact between the hot, reacted product gasses and the unburned portion of each grain. These two conditions make application of Frank-Kamanetskii laminar burn theory seem appropriate. Figure 13 shows that the anticipated burn velocities using the theory (Gill) are only a few-hundredths of a meter per second, over the range of experimental conditions. Clearly the theory, with room temperature properties, is inappropriate.

According to the theory, the dimensionless group upon which velocity depends is

$$V\left(\frac{T^{\ddagger}}{\alpha A \delta T}\right)^{1/2} = f \qquad (6)$$

where α is thermal diffusivity, δT the temperature rise

accompanying decomposition, A and $T^{\ddagger}$ are previously defined Arrhenius parameters and f is a rather weak function of some of the same variables and of the initial conditions. It is impossible for δT to vary much, being mostly controlled by the chemical bonding. Figure 14 shows that a considerably lower activation temperature would be required to elevate burn velocity to even 1 m/s, and this supposes the unburned material is at the unrealistically high average (not isentropic) temperature. However, numerical solution to the burn equations demonstrated that for $T^{\ddagger} < 6000$ K, burn waves were not steady and the rapid velocities achieved were more from a self-heating thermal explosion-like phenomenon than from a heat-transfer-dominated propagation.* Thus, in this range of properties, we computationally see a strong dependence of burn velocity on particle size, which is not observed in experiment. The only other property strongly affecting burn velocity is thermal diffusivity, which provides transport of thermal energy from hot to cold regions to ignite unburned material. While transport processes under shock loading have been studied very little, Bloomquist and Sheffield have postulated an increase in the thermal diffusivity by a factor of 10^4 in order to explain embedded thermocouple rise times in a shock-loaded organic material, PMMA. It is not known if such phenomena are operative here. If so, that should dramatically affect our perception of the decomposition process.

---

* We performed our own finite difference solutions to these problems which produced solutions which agreed that the F-K theoretical results in the steady burn regime, but which were capable of treating these non-steady cases.

VI. SUMMARY AND GENERAL REMARKS

We have compared a specific microstructural model with experimental observations on the decomposition history of shock-loaded porous HNS explosive. Hot-spot mass fraction is determined by the pore volume from which the hot spot was formed. Rapid hot-spot decomposition is definite evidence of enhanced reactivity. Velocities of subsequent laminar burn waves which propagate radially from each hot spot are observed to weakly depend upon the prevailing pressure, in contradiction with some current interpretations of data on other explosives, and are seen to be strongly dependent upon the initial shock pressure above a 2-GPa threshold. Velocities are very large compared with classical burn velocities and are independent of particle size and initial pressing density, within experimental resolution.

The nature of the results in this paper strongly suggest a general increase of reactivity of material which has been subjected to the shock environment. The reactivity change is dramatic within the highly disrupted hot spots and less dramatic in that material which is in the grain interior. There are also some indications that transport processes might be altered by this shock process. These general observations are in agreement with results of studies of chemical alteration produced by the shock process (Graham & Dodson). Some interpretations of the increase in reactivity produced by the shock process center on the high frequency content in the shock front and the attainment of a non-equilibrium temperature distribution which can be responsible for scissing particular chemical bonds (Dremin, Klimenko, Michailjuk & Trofimov).

Because the initially porous material under study here is very heterogeneous, shock rise times are relatively long and such high velocity gradients are not present on the molecular scale. That raises the possibility of alternative mechanisms to interpret the present experimental results. Bond-breaking which may accompany the large amount of plastic deformation occurring under shock-loading must be regarded as a candidate for explaining increase in reactivity seen in these experiments.

ACKNOWLEDGEMENT

This work has benefited from fruitful discussions with several colleagues. D. E. Mitchell, J. E. Kennedy, P. L. Stanton and J. W. Nunziato have been particularly helpful. Thanks are also due to C. M. Korbin who performed almost all of the numerous calculations cited here.

Figure Captions

Figure 1. Schematic of the experimental configuration. An HNS specimen (with fused-silica cover plate) impacts a fused-silica target with a thin embedded opaque metallic foil. Velocity interferometry measures the particle velocity history, which is used to infer the pressure history at the HNS/fused-silica interface.

Figure 2. Experimental records for experiments on HNS-I (equivalent spherical diameter of the grains of the bulk powder was 21 μm) pressed to initial density 1.60 Mg/m^3 (8.7% porosity) and shock loaded. See Table 1 for details. The particle velocity increase after t = 0.35 μs is identified with the pressure rise accompanying chemical decomposition.

Figure 3. Experimental records for HNS-I pressed to initial densities of 1.39 and 1.48 Mg/m^3. See Table 1 for details.

Figure 4. Experimental records for HNS-II (equivalent spherical diameter of powder grains of 37 μm) pressed to 1.60 Mg/m^3. See Table 1 for details.

Figure 5. Typical results from numerical simulation of disruption caused by shock-induced pore collapse.

(a) Initial pore shape at t = 1 ns. Note the isotherm, T = 342 K, is on the approaching shock; (b) Temperature distribution after shock passage at t = 4.25 ns. The pore is entirely collapsed. Contours start with T = 342 K (0.03 eV) which marks the shock front which has passed. All contours are separated by ΔT = 116 K (0.01 eV); (c) Comparison between actual distribution of temperature (expressed in terms of an equivalent spherical radius) and that obtained with a two-temperature model, using $W_H = \rho_o/\rho_{oo}-1$.

Figure 6. Results of two different numerical calculations on Experiment G9 showing empirical verification of the assumed proportionality between pressure rise after shock loading, and extent of decomposition. These two calculations, shown as dashed lines, were made using two different forms for the equation of state of the gaseous decomposition products. Also shown as a thin solid line is the calculated dependence of pressure rise on mass reaction decomposed, for an assumed steady wave propagating into the HNS.

Figure 7. Experiment G9 decomposition history showing two time regimes:

$t < 0.45$ μs, $x < 0.087 = W_H$; (hot-spots decompose).

$t > 0.45$ μs, $x > 0.087$; (grain burning consumes the material, with characteristic time $\tau_2 = 1.03$ μs).

Figure 8. Calculated hot-spot temperatures versus pressure for different initial pressing densities.

Figure 9. Measured delay times, τ_1, identified with the hot-spot decomposition time versus impact pressure.

Figure 10. Comparison of decomposition histories for specimens pressed from powder of different particle sizes. In experiment G4 and G9, HNS powders had grains with equivalent diameters of 20 μm and 37 μm, respectively. Similar decomposition histories for the first 0.4 μs are evidence that the dissipation process is self-similar on this scale, providing an upper bound on the scale length/time of the dissipation process. Later decomposition proceeds more rapidly in the "fine" material, which supports the observation that burn velocities are comparable.

Figure 11. Measured delay times versus hot-spot temperature. Extrapolated "ordinary" kinetics lead to calculations of much longer delays than those observed. If decomposition takes place through a self heating, thermal explosion process, kinetics must be greatly altered by the pore-collapse process.

Figure 12. Intragranular burn velocities as a function of impact pressure. Neither particle size nor initial pressing density seem to greatly affect the velocity.

Figure 13. Calculated burn velocity versus temperature of the unburned solid. That temperature results from isentropic compression, so that classical velocities are expected to be only 0.05 m/s at maximum.

Figure 14. Calculated burn velocity versus activation temperature $T^{\ddagger} = E^{\ddagger}/k$. For $T^{\ddagger} < 6000$ K, the F-K theory is no longer appropriate.

References

Anderson, A. B., Ginsberg, M. J., Seitz, W. L. and Wackerle, J. (1981) Shock initiation of porous TATB. Presented at the 7th Int. Symp. on Detonation, Annapolis, MD, U.S.A.

Barker, L. M. and Hollenbach, R. E., (1972) Laser interferometer for measuring high velocities of any reflecting surface. J. Appl. Phys., 43, p. 4669.

Bloomquist, D. D. and Sheffield, S. A. (1980) Thermocouple temperature in shock-compressed solids. J. Appl. Phys. 51 (10), pp. 5260-5266.

Bowden, F. P. and Yoffe, A. D. (1952) Initiation and growth of explosion in liquids and solids. Cambridge University Press, Cambridge, MA.

Butcher, B. M., Carroll, M. M. and Holt, A. C. (1974) Shock-wave compaction of porous aluminum. J. Appl. Phys. 45 (9), pp. 3864-3875.

Cowperthwaite, M. (1973) Determination of energy-release rate with the hydrodynamic properties of detonation waves. Proc. of the Fourteenth Symposium (International) on Combustion, The Combustion Institute, Pittsburgh, PA, pp. 1259-1264.

Dremin, A. N., Klimenko, V. Yu., Michailjuk, K. M. and Trofimov, V. S. (1981) On decomposition reaction kinetics in shock wave front. Proceedings of the 7th Int. Symp. on Detonation, Annapolis, MD, U.S.A. (to be published).

Dunin, S. Z. and Surkov, V. V. (1978) Structure of a shock wave front in a porous solid. Zhurnal Prikladnoi Mekhaniki i Tekhnicheskoi Fiziki No. 5, pp. 612-617.

Eyring, H., Powell, R. E., Duffey, G. H. and Parlin, R. B. (1949) The stability of detonation. Chem. Rev. 45, p. 69.

Forest, C. A. (1979) Initiation of heterogeneous explosives. A summary of C. A. Forest's model is given in Numerical Modeling of Detonations, by C. L. Mader, pp. 208-272 University of California Press, Ltd., Berkeley & Los Angeles, CA.

Gill, W. (1979) Frank-Kamenetskii revisited: flame ignition and propagation. Combustion and Flame 41, pp. 99-105.

Graham, R. A. and Dodson, B. W. (1980) Bibliography on shock induced chemistry. Sandia National Laboratories Report SAND80-1642.

Hayes, D. B. and Mitchell, D. E. (1978) A constitutive equation for the shock response of porous hexanitrostilbene (HNS) explosive. Proc. of the Symposium HDP, Commissariat á L'Energie Atomique, Paris, France, pp. 161-172.

Hayes, D. B., Mitchell, D. E., and Stanton, P. L., (1981) Shock induced chemical decomposition in HNS (to be published).

Kanel, G. I. (1978) Kinetics of the decomposition of cast TNT in shock waves. Translated from Fizika Goreniya i Vzryva 14, 1, pp. 113-117.

Kanel, G. I. and Dremin, A. N. (1977) Decomposition of cast trotyl in shock waves. Translated from Fizika Goreniya i Vzryva 13, 1, pp. 85-92.

Kennedy, J. E. (1970) Quartz gauge study of upstream reaction in a shocked explosive. Proc. of the Fifth Symposium (Int.) on Detonation, ONR Publication ACR-184, Pasadena, CA, August 1970, pp. 435-445.

Kennedy, J. E. and Nunziato, J. W. (1976) Shock-wave evolution in a chemically reacting solid. J. Mech. Phys. Solids, 24, pp. 107-124.

Kipp, M. E., Nunziato, J. W., Setchell, R. E. and Walsh, E. K. (1981) Hot spot initiation of heterogeneous explosives. Presented at the 7th Int. Symp. on Detonation, Annapolis, MD, U.S.A.

Lee, E. L. and Tarver, C. M. (1980) Phenomenological model of shock initiation in heterogeneous explosives. Phys. of Fluids 23 (12), pp. 2362-2372.

Mader, C. L. (1965) Initiation of detonation by the interaction of shocks with density discontinuities. Phys. of Fluids 8, (10), pp. 1811-1816.

Mitchell, D. E. and Hayes, D. B., (1981) An experimental investigation of shock-loaded HNS explosive (to be published).

Rogers, R. N., Los Alamos National Laboratory, private communication.

Schwarz, A. C. (1981) Study of factors which influence the shock-initiation sensitivity of hexanitrostilbene (HNS). Sandia National Laboratories Rpt. SAND80-2372.

Sheffield, S. A., Mitchell, D. E. and Hayes, D. B. (1976) The equation of state and chemical kinetics for hexanitrostilbene (HNS) explosive. Sixth Symp. (Int.) on Detonation, p. 748.

Thompson, S. A. (1979) CSQII -- An eulerian finite difference program for two-dimensional material response - Part 1. Material Sections. Sandia Laboratories Report SAND77-1339.

Wackerle, J., Rabie, R. L., Ginsberg, M. J. and Anderson, A. B., (1978) A shock initiation study of PBX-9404. Proc. of the Symposium HDP, Commissariat á L'Energie Atomique, Paris, France, pp. 127-138.

EXPERIMENTAL CONFIGURATION

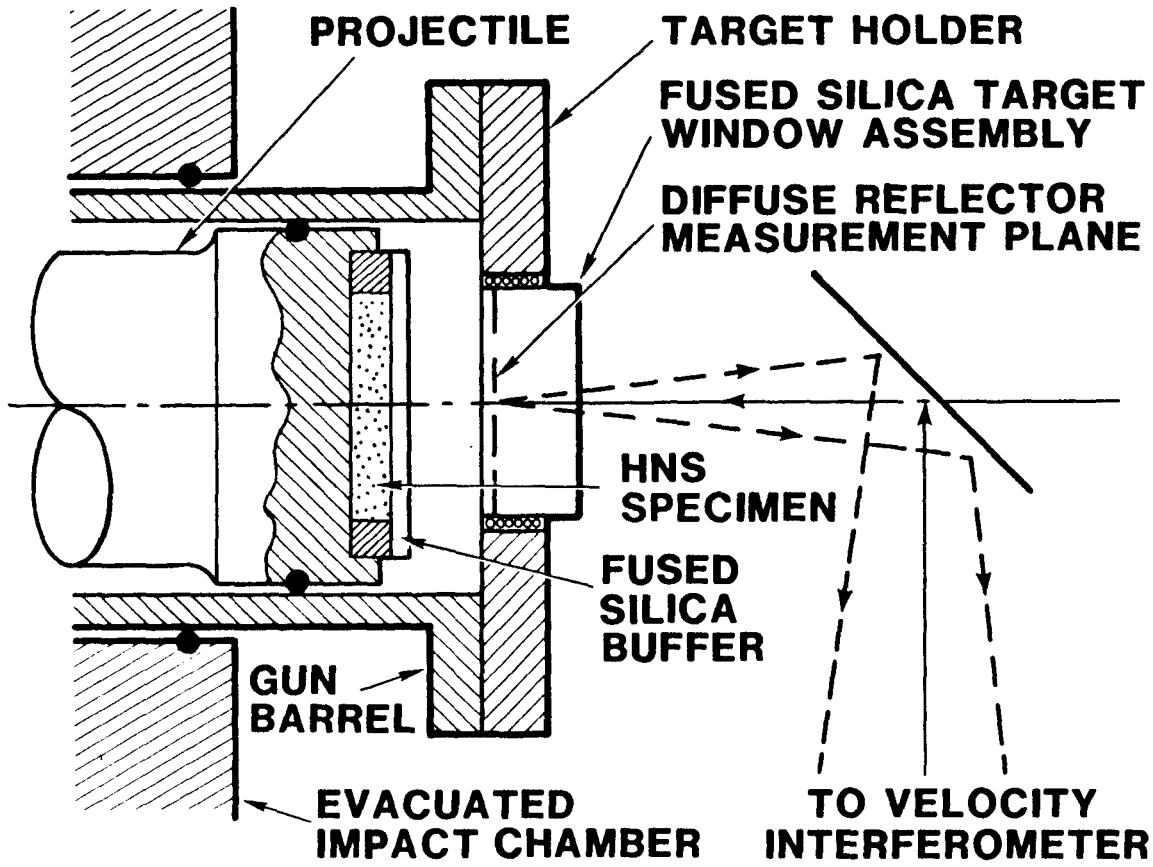

Sandia National Laboratories

Figure 1.

D. B. Hayes

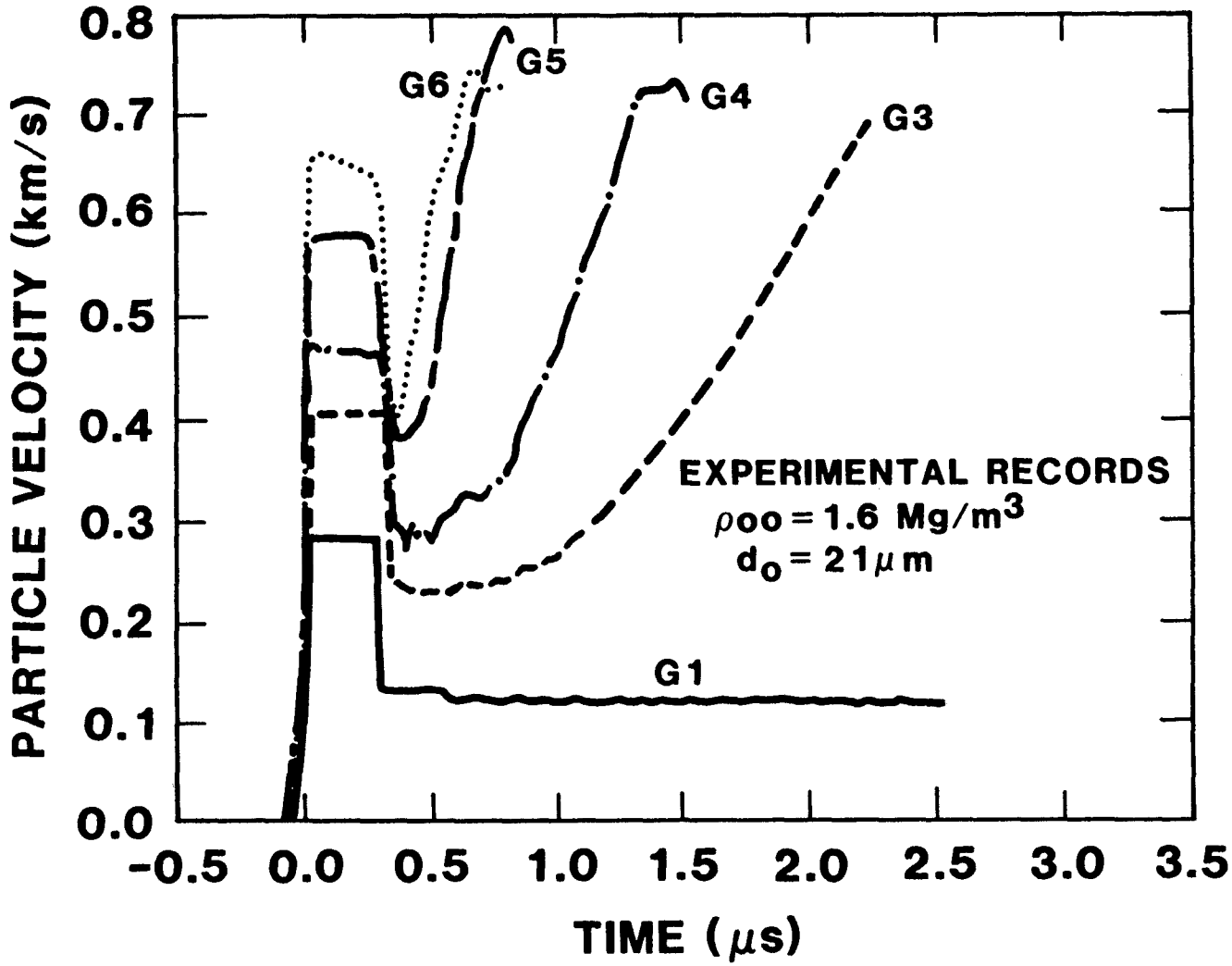

Sandia National Laboratories

Figure 2.

D. B. Hayes

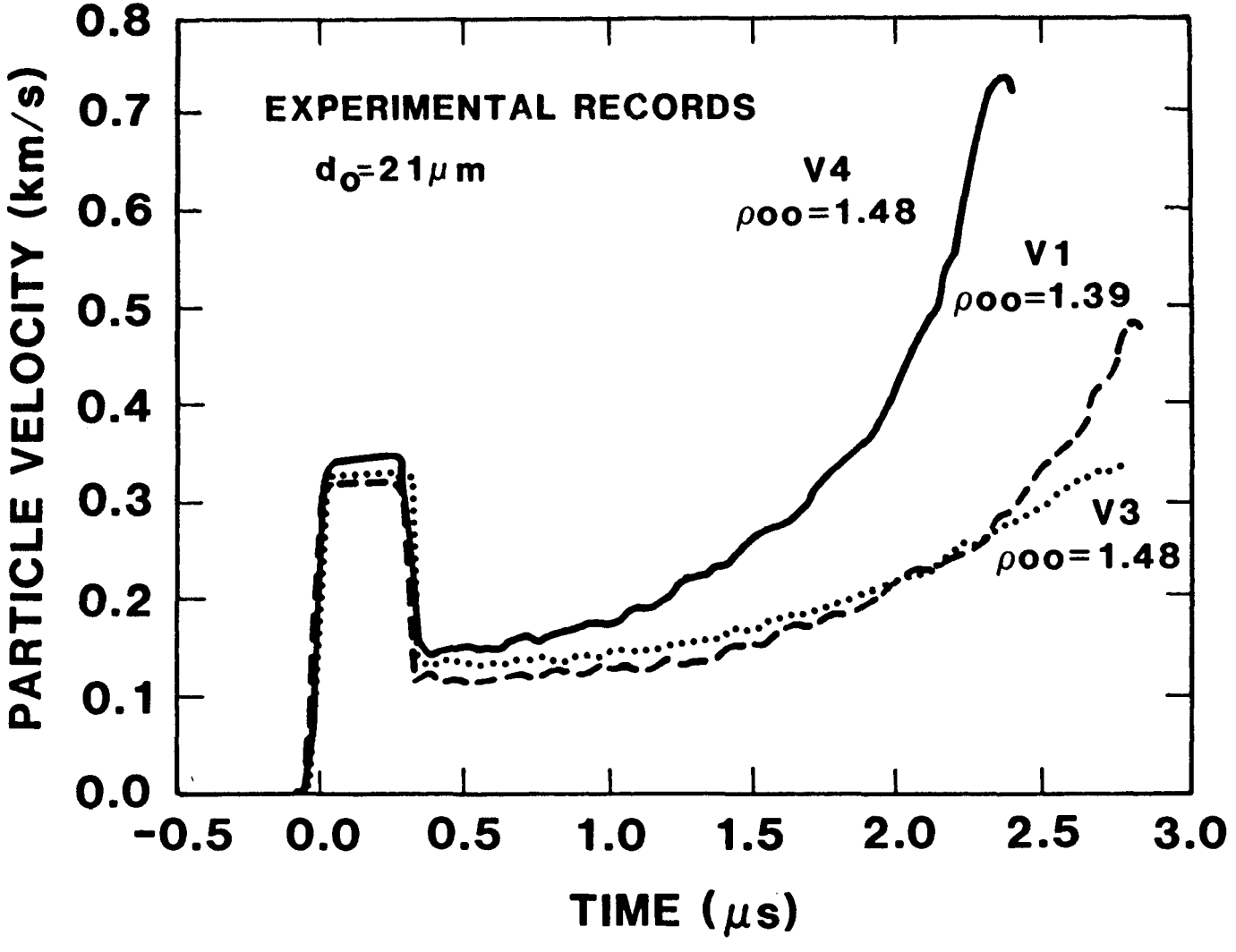

Figure 3.

D. B. Hayes

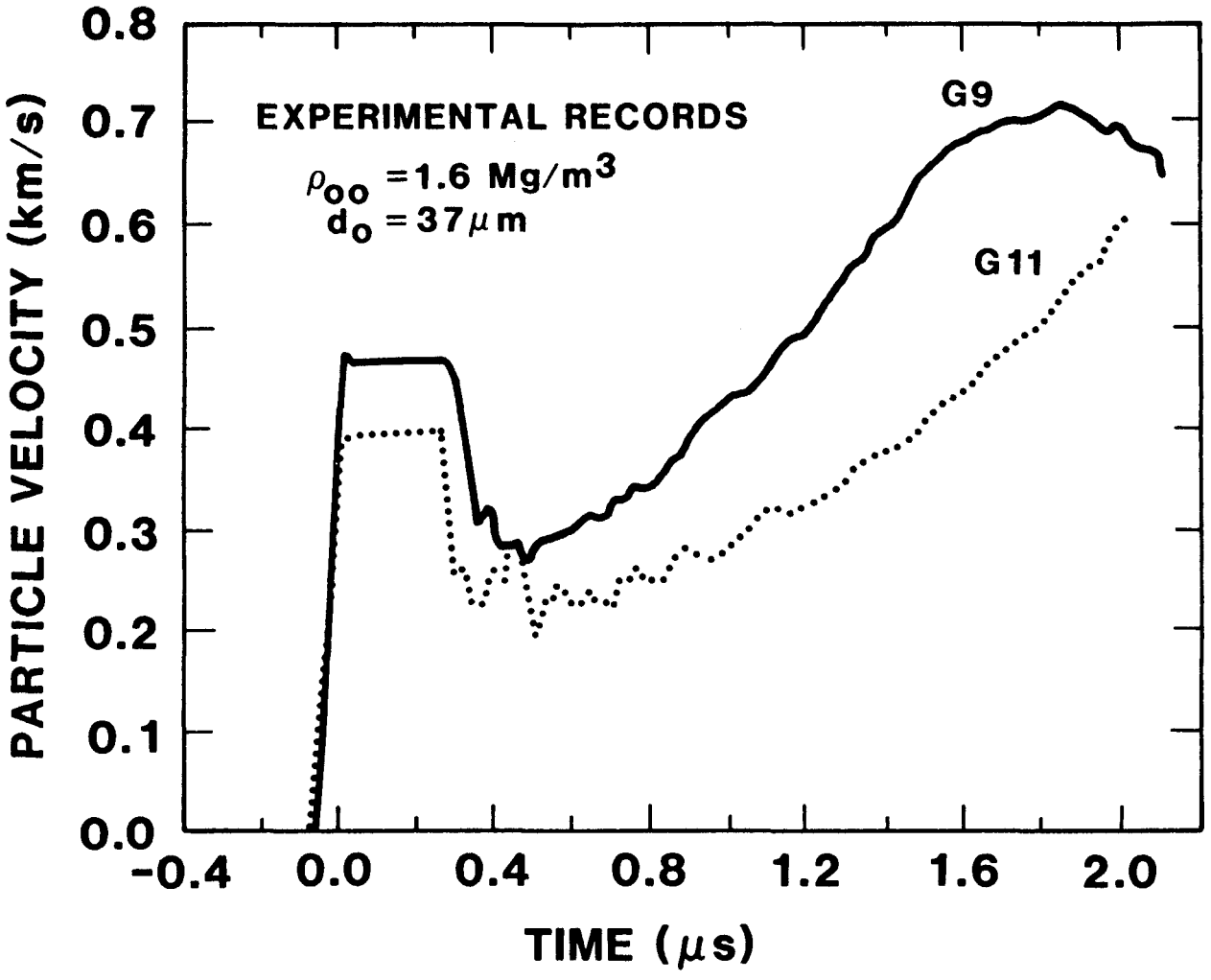

Sandia National Laboratories

Figure 4.

D. B. Hayes

HOT SPOT TEMPERATURE DISTRIBUTIONS
Po=3.3 GPa

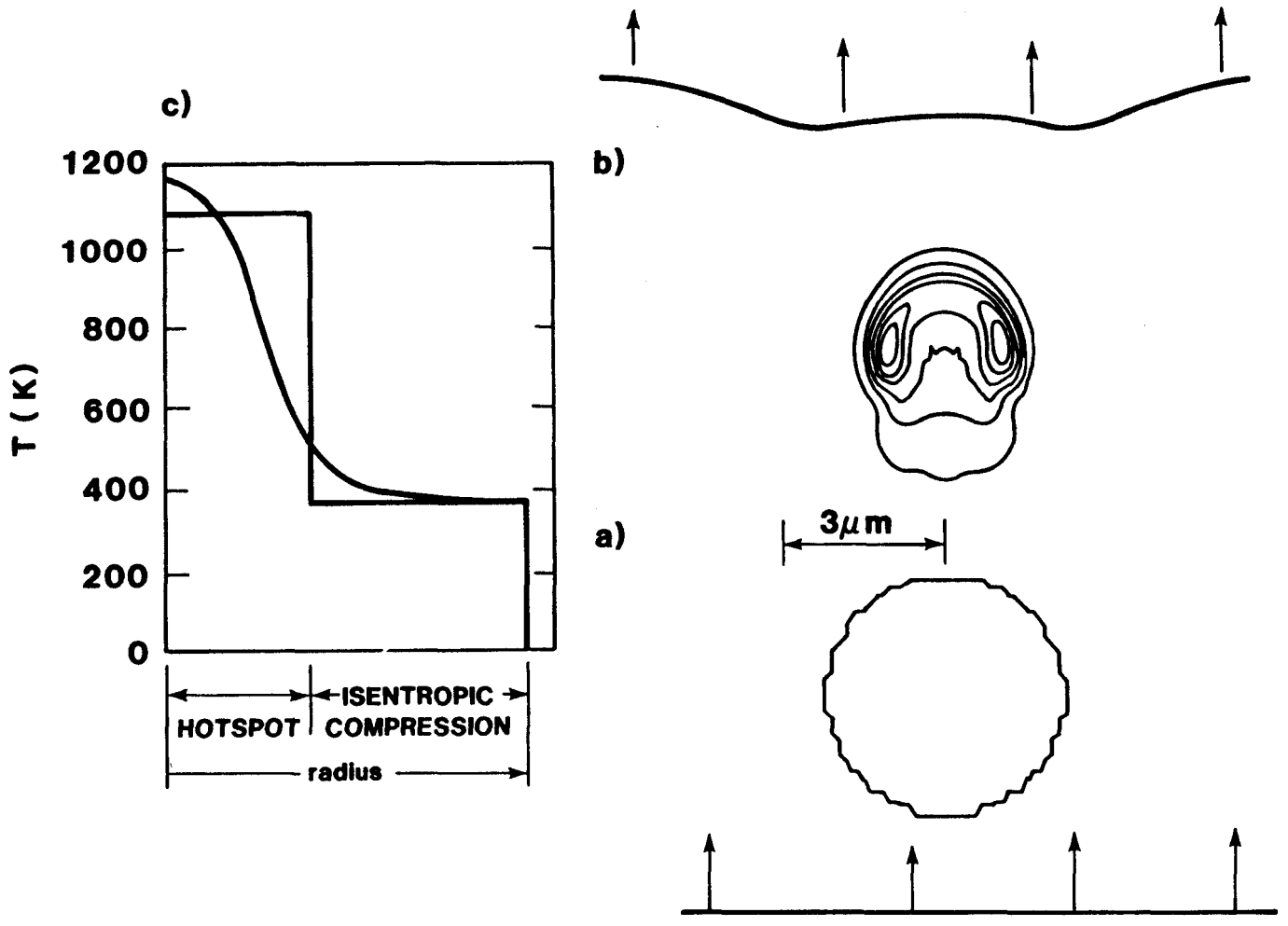

Figure 5.

D. B. Hayes

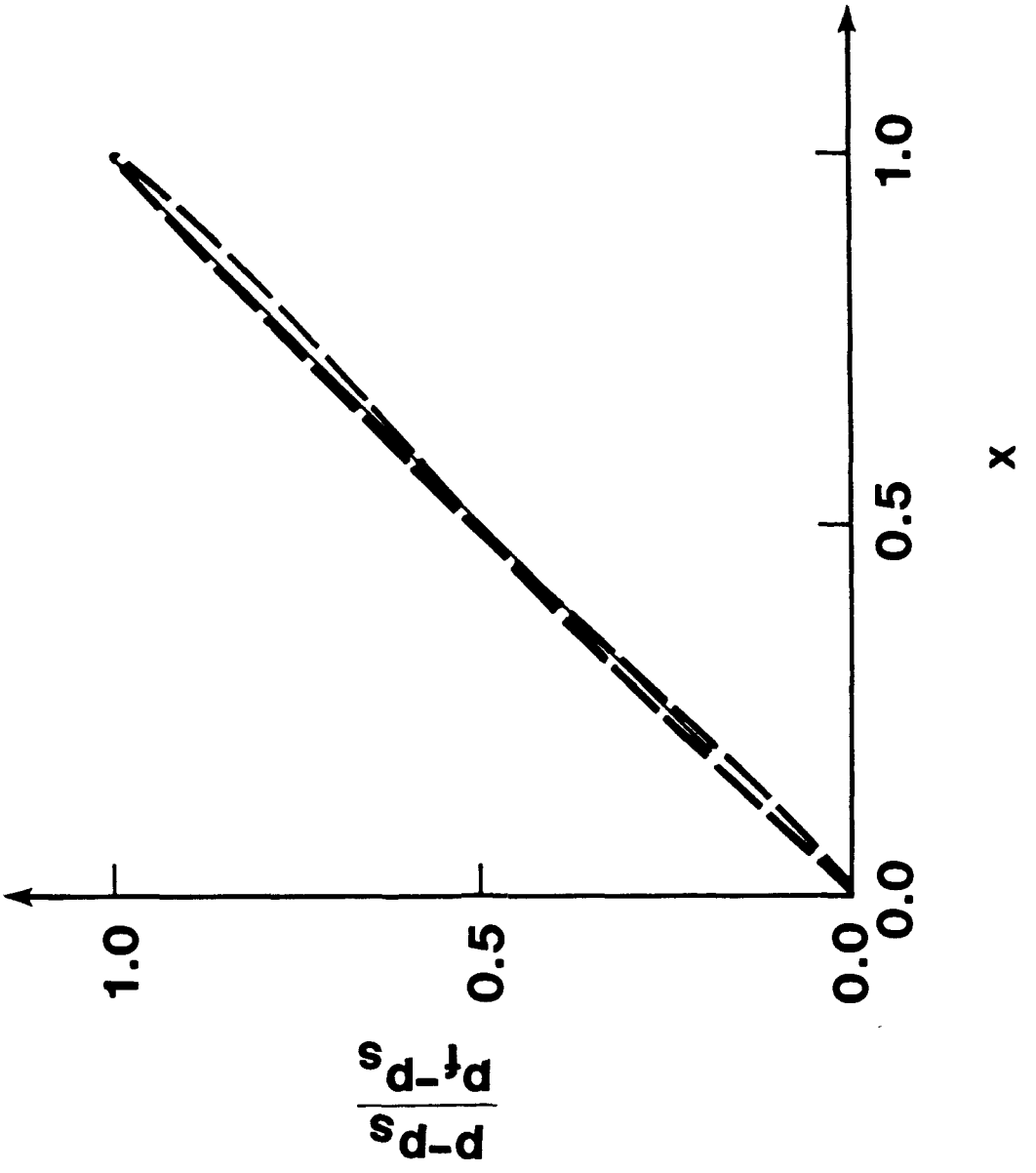

Sandia National Laboratories

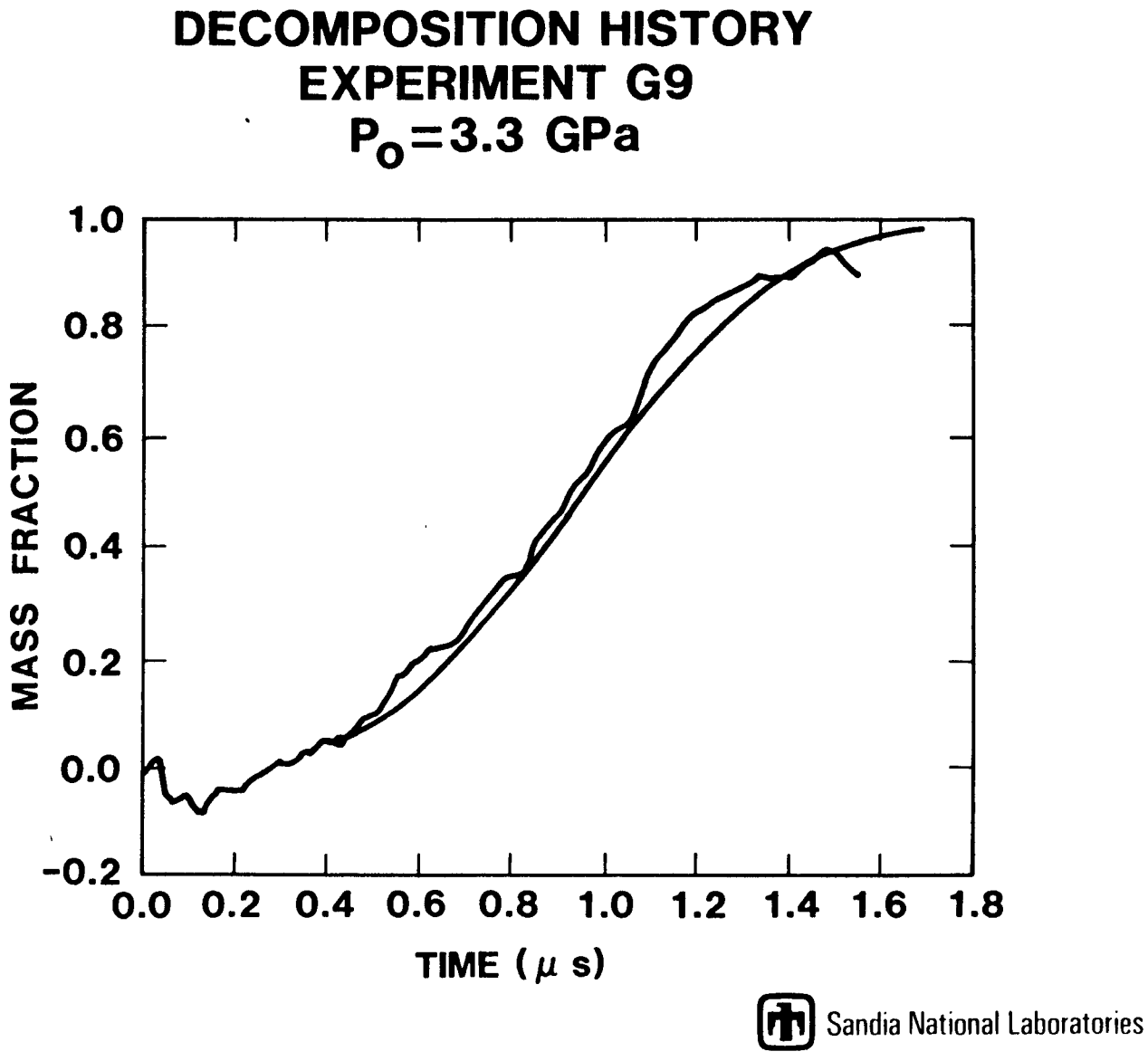

Figure 7.

D. B. Hayes

CALCULATED HOT SPOT TEMPERATURES

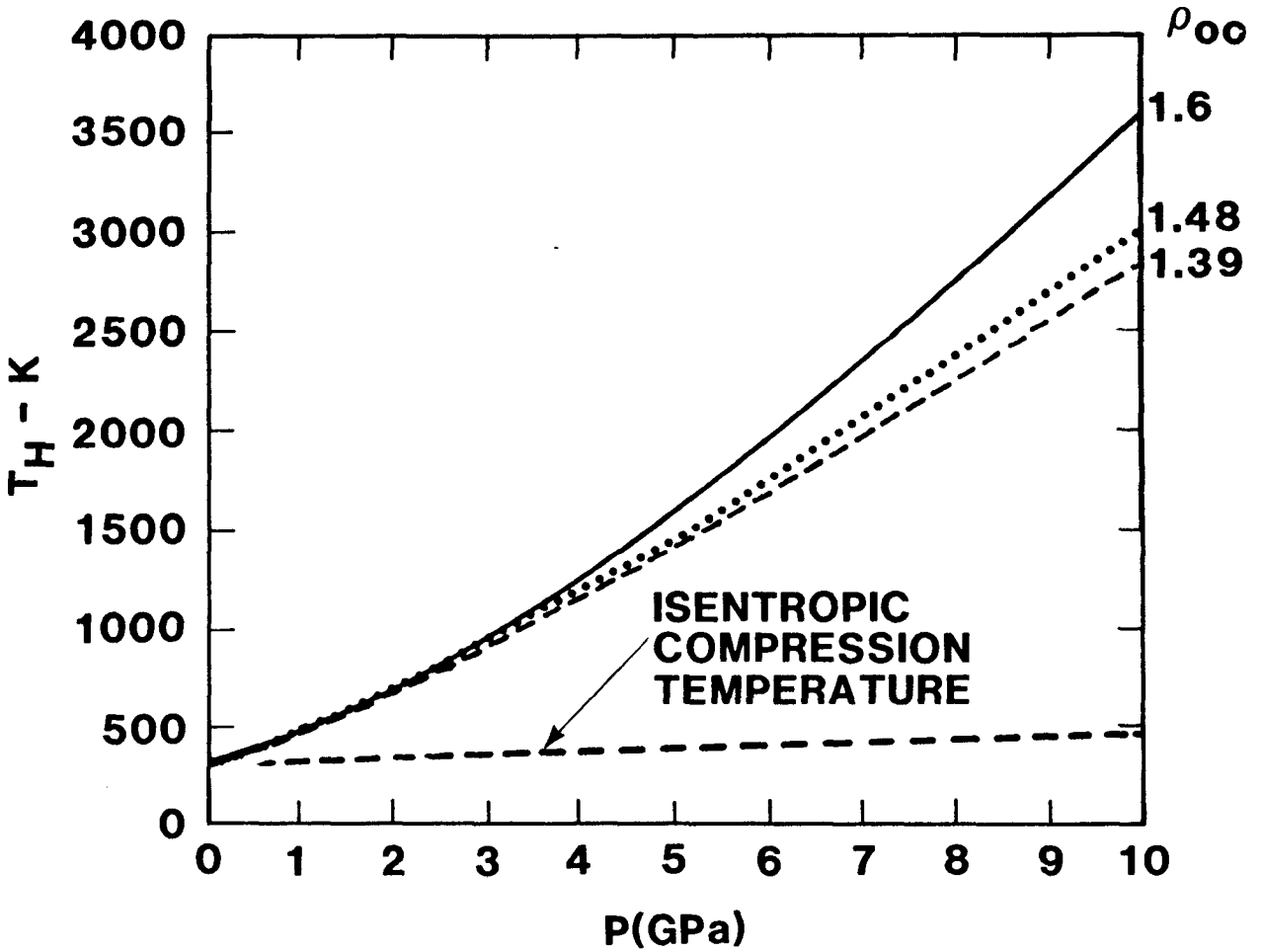

Sandia National Laboratories

Figure 8.

D. B. Hayes

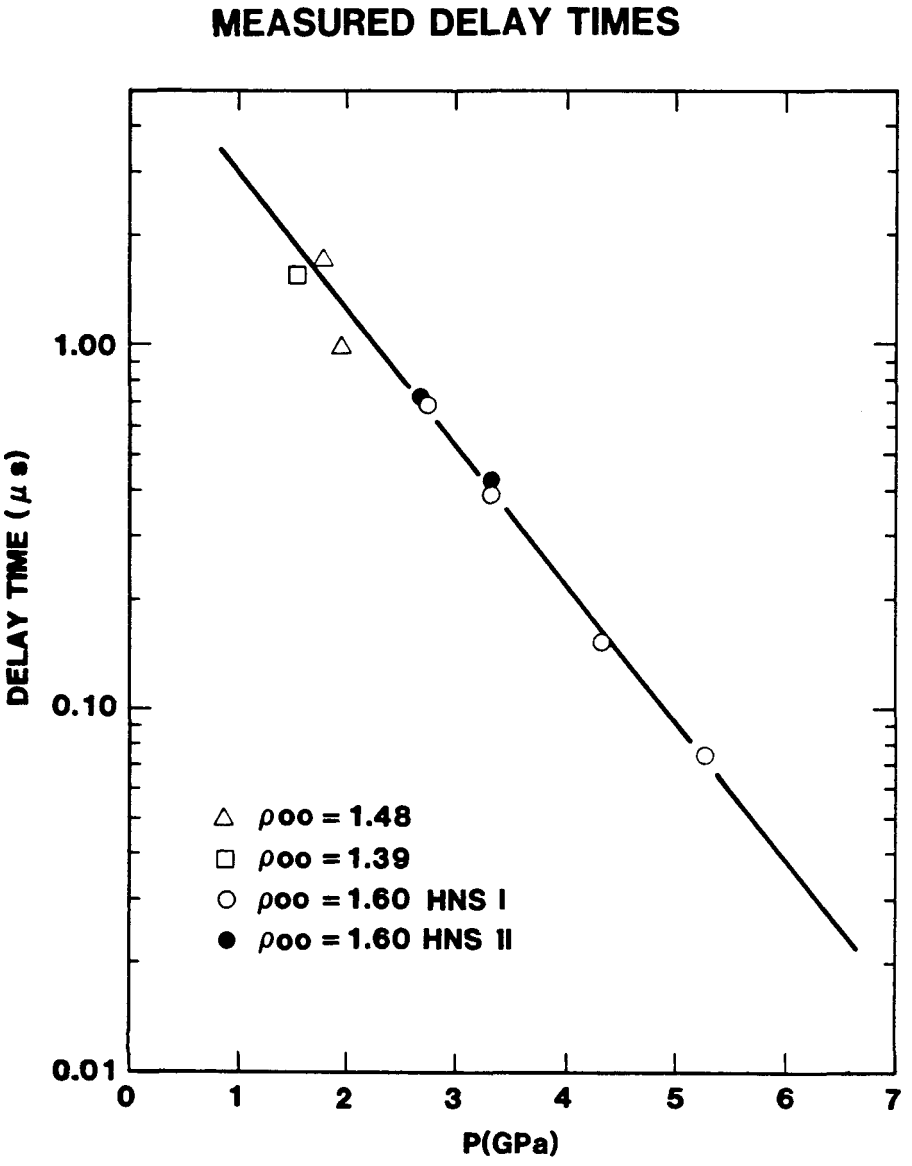
MEASURED DELAY TIMES
DELAY TIME (μ s)
1.00
0.10
0.01
0
1
2
3
4
5
6
7
P(GPa)
△ ρoo = 1.48
□ ρoo = 1.39
○ ρoo = 1.60 HNS I
● ρoo = 1.60 HNS II

DECOMPOSITION HISTORIES FOR EXPERIMENTS G4 AND G9

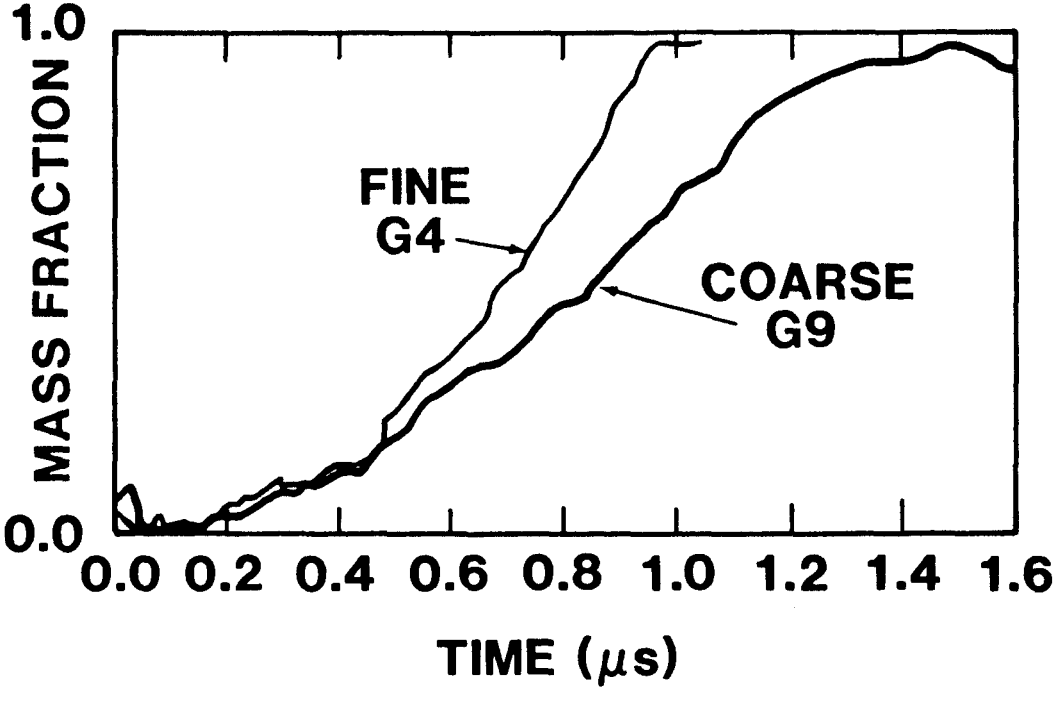

Sandia National Laboratories

Figure 10.

D. B. Hayes

Figure 11. D. B. Hayes

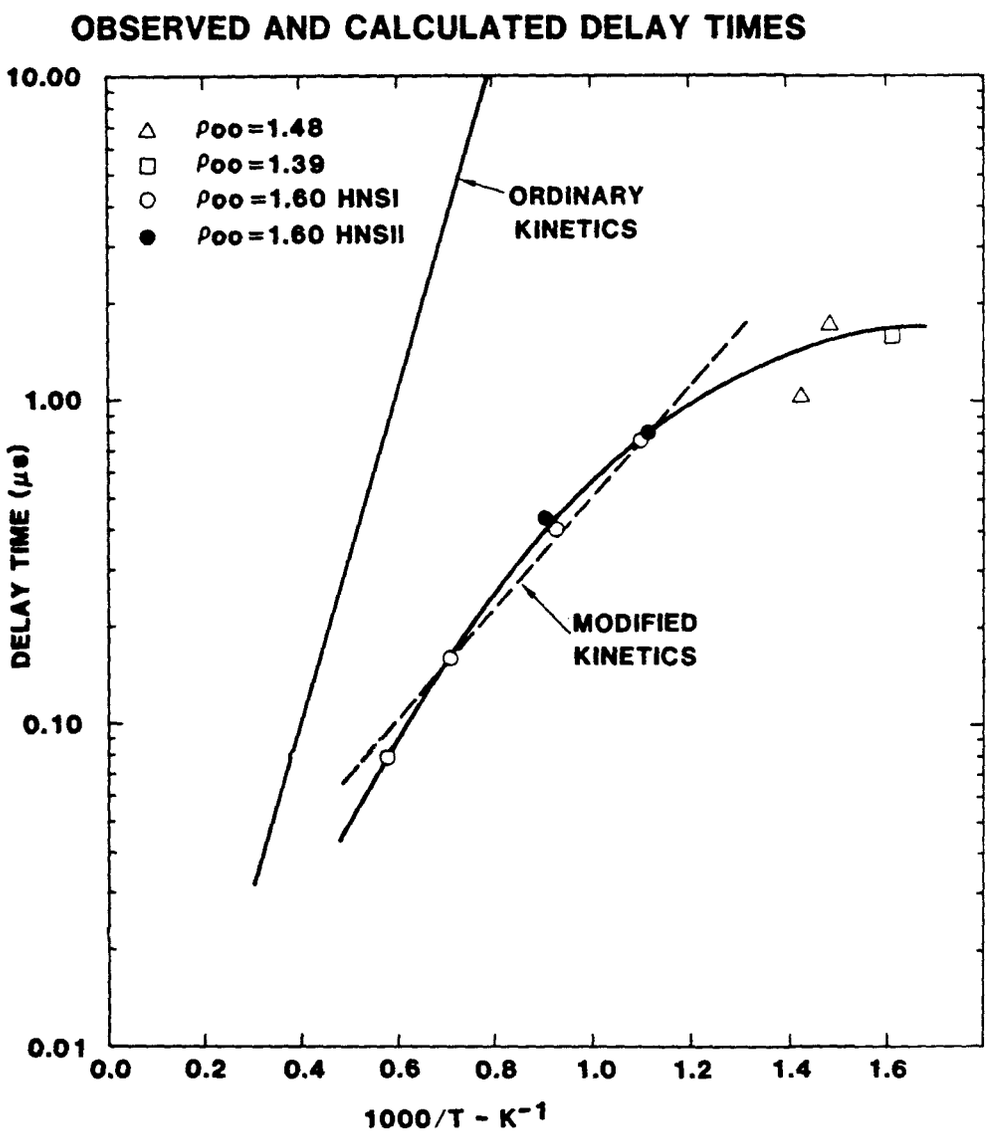

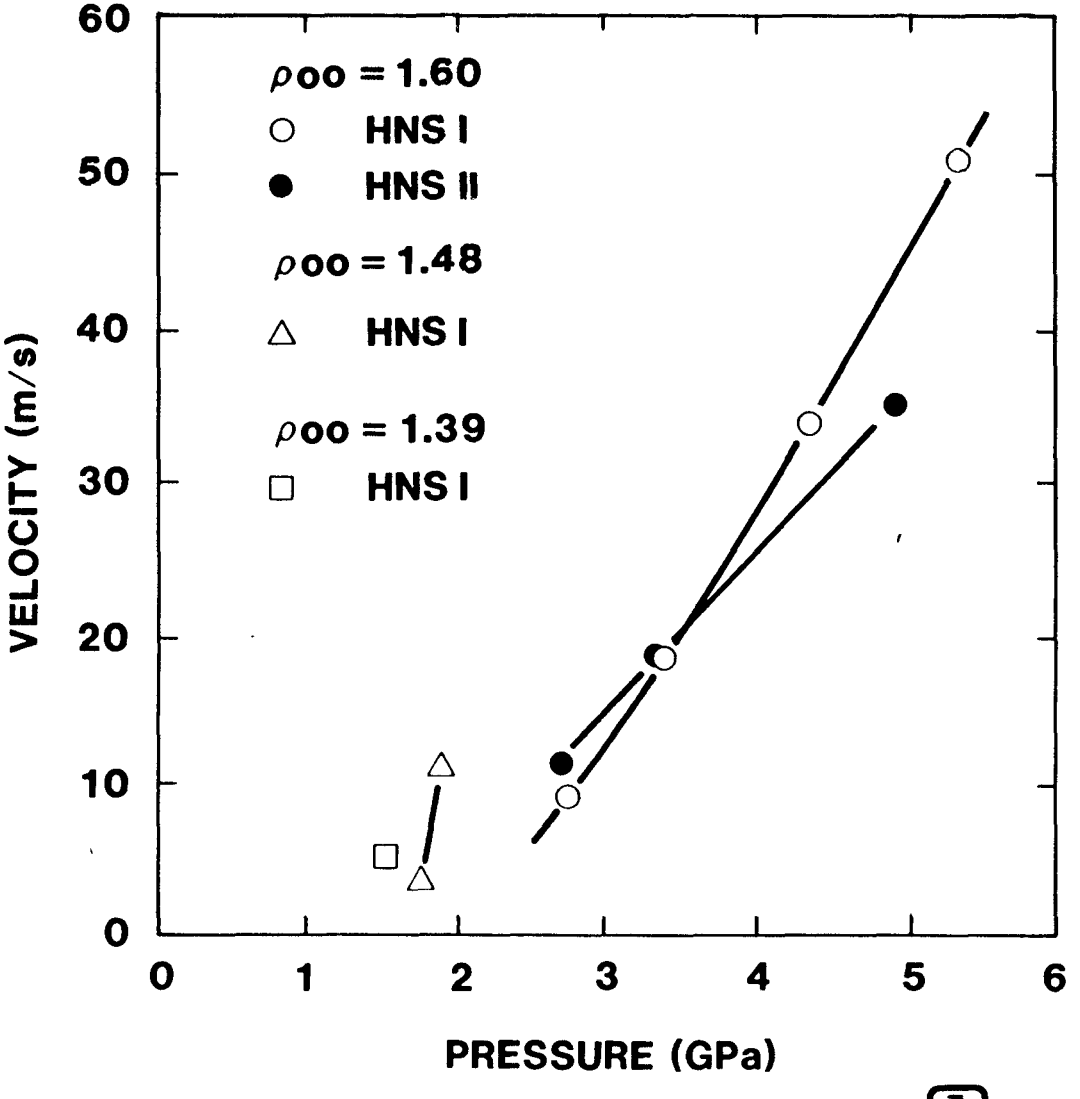

Sandia National Laboratories

Figure 12.

D. B. Hayes

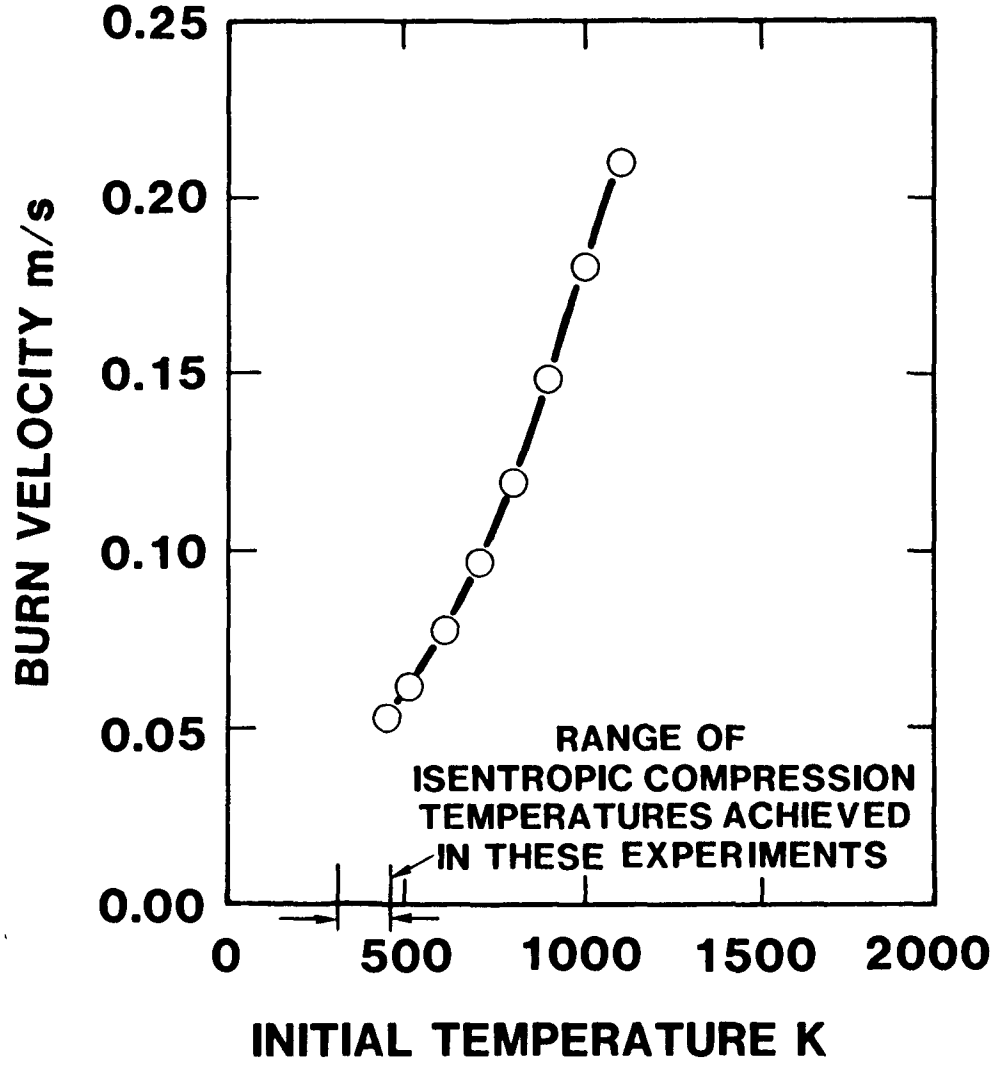

Sandia National Laboratories

Figure 13.

D. B. Hayes

EFFECT OF ACTIVATION TEMPERATURE ON BURN VELOCITY

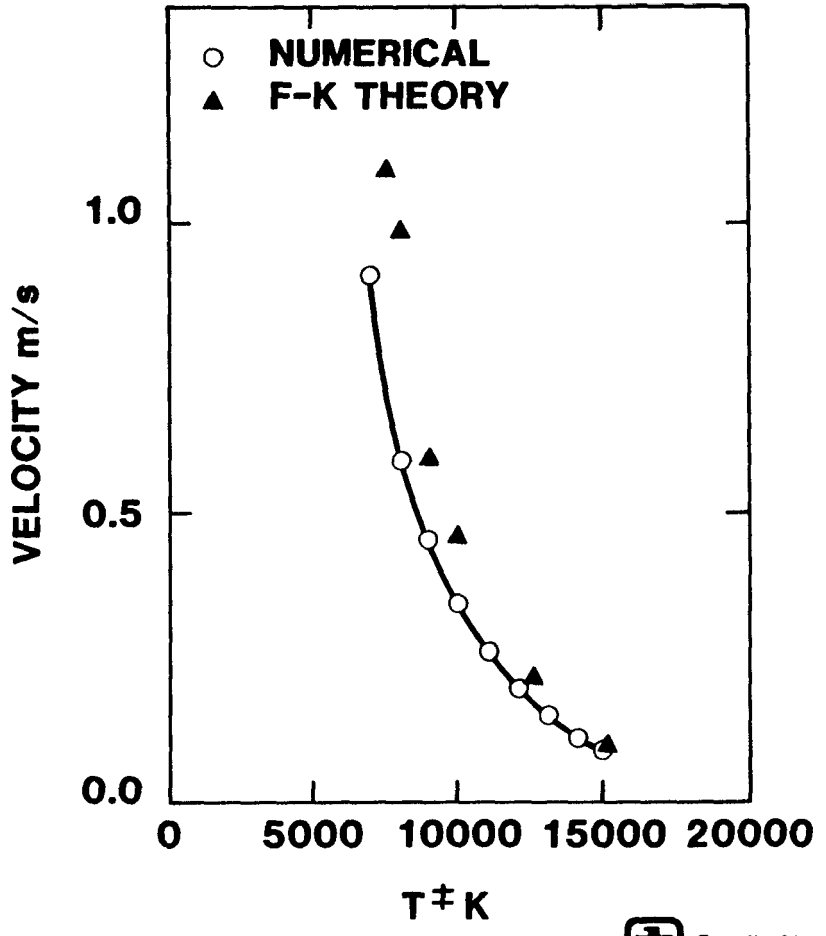

Sandia National Laboratories

Figure 14.

D. B. Hayes